Search for resonances decaying to $\eta_{c}\pi^{+}\pi^{-}$ in two-photon interactions

J. P. Lees *et al.* (BABAR Collaboration)

Phys. Rev. D **86**, 092005 — Published 6 November 2012

DOI: 10.1103/PhysRevD.86.092005

BaBar-PUB-12/004
SLAC-PUB-15052

Search for resonances decaying to $\eta_c \pi^+ \pi^-$ in two-photon interactions

J. P. Lees,[1] V. Poireau,[1] V. Tisserand,[1] J. Garra Tico,[2] E. Grauges,[2] A. Palano[ab],[3] G. Eigen,[4] B. Stugu,[4] D. N. Brown,[5] L. T. Kerth,[5] Yu. G. Kolomensky,[5] G. Lynch,[5] H. Koch,[6] T. Schroeder,[6] D. J. Asgeirsson,[7] C. Hearty,[7] T. S. Mattison,[7] J. A. McKenna,[7] R. Y. So,[7] A. Khan,[8] V. E. Blinov,[9] A. R. Buzykaev,[9] V. P. Druzhinin,[9] V. B. Golubev,[9] E. A. Kravchenko,[9] A. P. Onuchin,[9] S. I. Serednyakov,[9] Yu. I. Skovpen,[9] E. P. Solodov,[9] K. Yu. Todyshev,[9] A. N. Yushkov,[9] M. Bondioli,[10] D. Kirkby,[10] A. J. Lankford,[10] M. Mandelkern,[10] H. Atmacan,[11] J. W. Gary,[11] F. Liu,[11] O. Long,[11] G. M. Vitug,[11] C. Campagnari,[12] T. M. Hong,[12] D. Kovalskyi,[12] J. D. Richman,[12] C. A. West,[12] A. M. Eisner,[13] J. Kroseberg,[13] W. S. Lockman,[13] A. J. Martinez,[13] B. A. Schumm,[13] A. Seiden,[13] D. S. Chao,[14] C. H. Cheng,[14] B. Echenard,[14] K. T. Flood,[14] D. G. Hitlin,[14] P. Ongmongkolkul,[14] F. C. Porter,[14] A. Y. Rakitin,[14] R. Andreassen,[15] Z. Huard,[15] B. T. Meadows,[15] M. D. Sokoloff,[15] L. Sun,[15] P. C. Bloom,[16] W. T. Ford,[16] A. Gaz,[16] U. Nauenberg,[16] J. G. Smith,[16] S. R. Wagner,[16] R. Ayad,[17,*] W. H. Toki,[17] B. Spaan,[18] K. R. Schubert,[19] R. Schwierz,[19] D. Bernard,[20] M. Verderi,[20] P. J. Clark,[21] S. Playfer,[21] D. Bettoni[a],[22] C. Bozzi[a],[22] R. Calabrese[ab],[22] G. Cibinetto[ab],[22] E. Fioravanti[ab],[22] I. Garzia[ab],[22] E. Luppi[ab],[22] M. Munerato[ab],[22] M. Negrini[ab],[22] L. Piemontese[a],[22] V. Santoro[a],[22] R. Baldini-Ferroli,[23] A. Calcaterra,[23] R. de Sangro,[23] G. Finocchiaro,[23] P. Patteri,[23] I. M. Peruzzi,[23,†] M. Piccolo,[23] M. Rama,[23] A. Zallo,[23] R. Contri[ab],[24] E. Guido[ab],[24] M. Lo Vetere[ab],[24] M. R. Monge[ab],[24] S. Passaggio[a],[24] C. Patrignani[ab],[24] E. Robutti[a],[24] B. Bhuyan,[25] V. Prasad,[25] C. L. Lee,[26] M. Morii,[26] A. J. Edwards,[27] A. Adametz,[28] U. Uwer,[28] H. M. Lacker,[29] T. Lueck,[29] P. D. Dauncey,[30] P. K. Behera,[31] U. Mallik,[31] C. Chen,[32] J. Cochran,[32] W. T. Meyer,[32] S. Prell,[32] A. E. Rubin,[32] A. V. Gritsan,[33] Z. J. Guo,[33] N. Arnaud,[34] M. Davier,[34] D. Derkach,[34] G. Grosdidier,[34] F. Le Diberder,[34] A. M. Lutz,[34] B. Malaescu,[34] P. Roudeau,[34] M. H. Schune,[34] A. Stocchi,[34] G. Wormser,[34] D. J. Lange,[35] D. M. Wright,[35] C. A. Chavez,[36] J. P. Coleman,[36] J. R. Fry,[36] E. Gabathuler,[36] D. E. Hutchcroft,[36] D. J. Payne,[36] C. Touramanis,[36] A. J. Bevan,[37] F. Di Lodovico,[37] R. Sacco,[37] M. Sigamani,[37] G. Cowan,[38] D. N. Brown,[39] C. L. Davis,[39] A. G. Denig,[40] M. Fritsch,[40] W. Gradl,[40] K. Griessinger,[40] A. Hafner,[40] E. Prencipe,[40] R. J. Barlow,[41,‡] G. Jackson,[41] G. D. Lafferty,[41] E. Behn,[42] R. Cenci,[42] B. Hamilton,[42] A. Jawahery,[42] D. A. Roberts,[42] C. Dallapiccola,[43] R. Cowan,[44] D. Dujmic,[44] G. Sciolla,[44] R. Cheaib,[45] D. Lindemann,[45] P. M. Patel,[45] S. H. Robertson,[45] P. Biassoni[ab],[46] N. Neri[a],[46] F. Palombo[ab],[46] S. Stracka[ab],[46] L. Cremaldi,[47] R. Godang,[47,§] R. Kroeger,[47] P. Sonnek,[47] D. J. Summers,[47] X. Nguyen,[48] M. Simard,[48] P. Taras,[48] G. De Nardo[ab],[49] D. Monorchio[ab],[49] G. Onorato[ab],[49] C. Sciacca[ab],[49] M. Martinelli,[50] G. Raven,[50] C. P. Jessop,[51] J. M. LoSecco,[51] W. F. Wang,[51] K. Honscheid,[52] R. Kass,[52] J. Brau,[53] R. Frey,[53] N. B. Sinev,[53] D. Strom,[53] E. Torrence,[53] E. Feltresi[ab],[54] N. Gagliardi[ab],[54] M. Margoni[ab],[54] M. Morandin[a],[54] M. Posocco[a],[54] M. Rotondo[a],[54] G. Simi[a],[54] F. Simonetto[ab],[54] R. Stroili[ab],[54] S. Akar,[55] E. Ben-Haim,[55] M. Bomben,[55] G. R. Bonneaud,[55] H. Briand,[55] G. Calderini,[55] J. Chauveau,[55] O. Hamon,[55] Ph. Leruste,[55] G. Marchiori,[55] J. Ocariz,[55] S. Sitt,[55] M. Biasini[ab],[56] E. Manoni[ab],[56] S. Pacetti[ab],[56] A. Rossi[ab],[56] C. Angelini[ab],[57] G. Batignani[ab],[57] S. Bettarini[ab],[57] M. Carpinelli[ab],[57,¶] G. Casarosa[ab],[57] A. Cervelli[ab],[57] F. Forti[ab],[57] M. A. Giorgi[ab],[57] A. Lusiani[ac],[57] B. Oberhof[ab],[57] E. Paoloni[ab],[57] A. Perez[a],[57] G. Rizzo[ab],[57] J. J. Walsh[a],[57] D. Lopes Pegna,[58] J. Olsen,[58] A. J. S. Smith,[58] A. V. Telnov,[58] F. Anulli[a],[59] R. Faccini[ab],[59] F. Ferrarotto[a],[59] F. Ferroni[ab],[59] M. Gaspero[ab],[59] L. Li Gioi[a],[59] M. A. Mazzoni[a],[59] G. Piredda[a],[59] C. Bünger,[60] O. Grünberg,[60] T. Hartmann,[60] T. Leddig,[60] H. Schröder,[60,**] C. Voss,[60] R. Waldi,[60] T. Adye,[61] E. O. Olaiya,[61] F. F. Wilson,[61] S. Emery,[62] G. Hamel de Monchenault,[62] G. Vasseur,[62] Ch. Yèche,[62] D. Aston,[63] D. J. Bard,[63] R. Bartoldus,[63] J. F. Benitez,[63] C. Cartaro,[63] M. R. Convery,[63] J. Dorfan,[63] G. P. Dubois-Felsmann,[63] W. Dunwoodie,[63] M. Ebert,[63] R. C. Field,[63] M. Franco Sevilla,[63] B. G. Fulsom,[63] A. M. Gabareen,[63] M. T. Graham,[63] P. Grenier,[63] C. Hast,[63] W. R. Innes,[63] M. H. Kelsey,[63] P. Kim,[63] M. L. Kocian,[63] D. W. G. S. Leith,[63] P. Lewis,[63] B. Lindquist,[63] S. Luitz,[63] V. Luth,[63] H. L. Lynch,[63] D. B. MacFarlane,[63] D. R. Muller,[63] H. Neal,[63] S. Nelson,[63] M. Perl,[63] T. Pulliam,[63] B. N. Ratcliff,[63] A. Roodman,[63] A. A. Salnikov,[63] R. H. Schindler,[63] A. Snyder,[63] D. Su,[63] M. K. Sullivan,[63] J. Va'vra,[63] A. P. Wagner,[63] W. J. Wisniewski,[63] M. Wittgen,[63] D. H. Wright,[63] H. W. Wulsin,[63] C. C. Young,[63] V. Ziegler,[63] W. Park,[64] M. V. Purohit,[64] R. M. White,[64] J. R. Wilson,[64] A. Randle-Conde,[65] S. J. Sekula,[65] M. Bellis,[66] P. R. Burchat,[66] T. S. Miyashita,[66] M. S. Alam,[67] J. A. Ernst,[67] R. Gorodeisky,[68] N. Guttman,[68] D. R. Peimer,[68] A. Soffer,[68] P. Lund,[69] S. M. Spanier,[69] J. L. Ritchie,[70] A. M. Ruland,[70] R. F. Schwitters,[70] B. C. Wray,[70] J. M. Izen,[71] X. C. Lou,[71] F. Bianchi[ab],[72] D. Gamba[ab],[72] L. Lanceri[ab],[73] L. Vitale[ab],[73] F. Martinez-Vidal,[74] A. Oyanguren,[74]

H. Ahmed,[75] J. Albert,[75] Sw. Banerjee,[75] F. U. Bernlochner,[75] H. H. F. Choi,[75] G. J. King,[75] R. Kowalewski,[75] M. J. Lewczuk,[75] I. M. Nugent,[75] J. M. Roney,[75] R. J. Sobie,[75] N. Tasneem,[75] T. J. Gershon,[76] P. F. Harrison,[76] T. E. Latham,[76] E. M. T. Puccio,[76] H. R. Band,[77] S. Dasu,[77] Y. Pan,[77] R. Prepost,[77] and S. L. Wu[77]

(The *BABAR* Collaboration)

[1]*Laboratoire d'Annecy-le-Vieux de Physique des Particules (LAPP), Université de Savoie, CNRS/IN2P3, F-74941 Annecy-Le-Vieux, France*

[2]*Universitat de Barcelona, Facultat de Fisica, Departament ECM, E-08028 Barcelona, Spain*

[3]*INFN Sezione di Bari[a]; Dipartimento di Fisica, Università di Bari[b], I-70126 Bari, Italy*

[4]*University of Bergen, Institute of Physics, N-5007 Bergen, Norway*

[5]*Lawrence Berkeley National Laboratory and University of California, Berkeley, California 94720, USA*

[6]*Ruhr Universität Bochum, Institut für Experimentalphysik 1, D-44780 Bochum, Germany*

[7]*University of British Columbia, Vancouver, British Columbia, Canada V6T 1Z1*

[8]*Brunel University, Uxbridge, Middlesex UB8 3PH, United Kingdom*

[9]*Budker Institute of Nuclear Physics, Novosibirsk 630090, Russia*

[10]*University of California at Irvine, Irvine, California 92697, USA*

[11]*University of California at Riverside, Riverside, California 92521, USA*

[12]*University of California at Santa Barbara, Santa Barbara, California 93106, USA*

[13]*University of California at Santa Cruz, Institute for Particle Physics, Santa Cruz, California 95064, USA*

[14]*California Institute of Technology, Pasadena, California 91125, USA*

[15]*University of Cincinnati, Cincinnati, Ohio 45221, USA*

[16]*University of Colorado, Boulder, Colorado 80309, USA*

[17]*Colorado State University, Fort Collins, Colorado 80523, USA*

[18]*Technische Universität Dortmund, Fakultät Physik, D-44221 Dortmund, Germany*

[19]*Technische Universität Dresden, Institut für Kern- und Teilchenphysik, D-01062 Dresden, Germany*

[20]*Laboratoire Leprince-Ringuet, Ecole Polytechnique, CNRS/IN2P3, F-91128 Palaiseau, France*

[21]*University of Edinburgh, Edinburgh EH9 3JZ, United Kingdom*

[22]*INFN Sezione di Ferrara[a]; Dipartimento di Fisica, Università di Ferrara[b], I-44100 Ferrara, Italy*

[23]*INFN Laboratori Nazionali di Frascati, I-00044 Frascati, Italy*

[24]*INFN Sezione di Genova[a]; Dipartimento di Fisica, Università di Genova[b], I-16146 Genova, Italy*

[25]*Indian Institute of Technology Guwahati, Guwahati, Assam, 781 039, India*

[26]*Harvard University, Cambridge, Massachusetts 02138, USA*

[27]*Harvey Mudd College, Claremont, California 91711*

[28]*Universität Heidelberg, Physikalisches Institut, Philosophenweg 12, D-69120 Heidelberg, Germany*

[29]*Humboldt-Universität zu Berlin, Institut für Physik, Newtonstr. 15, D-12489 Berlin, Germany*

[30]*Imperial College London, London, SW7 2AZ, United Kingdom*

[31]*University of Iowa, Iowa City, Iowa 52242, USA*

[32]*Iowa State University, Ames, Iowa 50011-3160, USA*

[33]*Johns Hopkins University, Baltimore, Maryland 21218, USA*

[34]*Laboratoire de l'Accélérateur Linéaire, IN2P3/CNRS et Université Paris-Sud 11, Centre Scientifique d'Orsay, B. P. 34, F-91898 Orsay Cedex, France*

[35]*Lawrence Livermore National Laboratory, Livermore, California 94550, USA*

[36]*University of Liverpool, Liverpool L69 7ZE, United Kingdom*

[37]*Queen Mary, University of London, London, E1 4NS, United Kingdom*

[38]*University of London, Royal Holloway and Bedford New College, Egham, Surrey TW20 0EX, United Kingdom*

[39]*University of Louisville, Louisville, Kentucky 40292, USA*

[40]*Johannes Gutenberg-Universität Mainz, Institut für Kernphysik, D-55099 Mainz, Germany*

[41]*University of Manchester, Manchester M13 9PL, United Kingdom*

[42]*University of Maryland, College Park, Maryland 20742, USA*

[43]*University of Massachusetts, Amherst, Massachusetts 01003, USA*

[44]*Massachusetts Institute of Technology, Laboratory for Nuclear Science, Cambridge, Massachusetts 02139, USA*

[45]*McGill University, Montréal, Québec, Canada H3A 2T8*

[46]*INFN Sezione di Milano[a]; Dipartimento di Fisica, Università di Milano[b], I-20133 Milano, Italy*

[47]*University of Mississippi, University, Mississippi 38677, USA*

[48]*Université de Montréal, Physique des Particules, Montréal, Québec, Canada H3C 3J7*

[49]*INFN Sezione di Napoli[a]; Dipartimento di Scienze Fisiche, Università di Napoli Federico II[b], I-80126 Napoli, Italy*

[50]*NIKHEF, National Institute for Nuclear Physics and High Energy Physics, NL-1009 DB Amsterdam, The Netherlands*

[51]*University of Notre Dame, Notre Dame, Indiana 46556, USA*

[52]*Ohio State University, Columbus, Ohio 43210, USA*

[53]*University of Oregon, Eugene, Oregon 97403, USA*

[54]*INFN Sezione di Padova[a]; Dipartimento di Fisica, Università di Padova[b], I-35131 Padova, Italy*

[55]Laboratoire de Physique Nucléaire et de Hautes Energies,
IN2P3/CNRS, Université Pierre et Marie Curie-Paris6,
Université Denis Diderot-Paris7, F-75252 Paris, France
[56]INFN Sezione di Perugia[a]; Dipartimento di Fisica, Università di Perugia[b], I-06100 Perugia, Italy
[57]INFN Sezione di Pisa[a]; Dipartimento di Fisica,
Università di Pisa[b]; Scuola Normale Superiore di Pisa[c], I-56127 Pisa, Italy
[58]Princeton University, Princeton, New Jersey 08544, USA
[59]INFN Sezione di Roma[a]; Dipartimento di Fisica,
Università di Roma La Sapienza[b], I-00185 Roma, Italy
[60]Universität Rostock, D-18051 Rostock, Germany
[61]Rutherford Appleton Laboratory, Chilton, Didcot, Oxon, OX11 0QX, United Kingdom
[62]CEA, Irfu, SPP, Centre de Saclay, F-91191 Gif-sur-Yvette, France
[63]SLAC National Accelerator Laboratory, Stanford, California 94309 USA
[64]University of South Carolina, Columbia, South Carolina 29208, USA
[65]Southern Methodist University, Dallas, Texas 75275, USA
[66]Stanford University, Stanford, California 94305-4060, USA
[67]State University of New York, Albany, New York 12222, USA
[68]Tel Aviv University, School of Physics and Astronomy, Tel Aviv, 69978, Israel
[69]University of Tennessee, Knoxville, Tennessee 37996, USA
[70]University of Texas at Austin, Austin, Texas 78712, USA
[71]University of Texas at Dallas, Richardson, Texas 75083, USA
[72]INFN Sezione di Torino[a]; Dipartimento di Fisica Sperimentale, Università di Torino[b], I-10125 Torino, Italy
[73]INFN Sezione di Trieste[a]; Dipartimento di Fisica, Università di Trieste[b], I-34127 Trieste, Italy
[74]IFIC, Universitat de Valencia-CSIC, E-46071 Valencia, Spain
[75]University of Victoria, Victoria, British Columbia, Canada V8W 3P6
[76]Department of Physics, University of Warwick, Coventry CV4 7AL, United Kingdom
[77]University of Wisconsin, Madison, Wisconsin 53706, USA

We report a study of the process $\gamma\gamma \to X \to \eta_c \pi^+\pi^-$, where X stands for one of the resonances $\chi_{c2}(1P)$, $\eta_c(2S)$, $X(3872)$, $X(3915)$, or $\chi_{c2}(2P)$. The analysis is performed with a data sample of 473.9 fb^{-1} collected with the *BABAR* detector at the PEP-II asymmetric-energy electron-positron collider. We do not observe a significant signal for any channel, and calculate 90% confidence-level upper limits on the products of branching fractions and two-photon widths $\Gamma_{X\to\gamma\gamma}\mathcal{B}(X \to \eta_c\pi^+\pi^-)$: 15.7 eV for $\chi_{c2}(1P)$, 133 eV for $\eta_c(2S)$, 11.1 eV for $X(3872)$ (assuming it to be a spin-2 state), 16 eV for $X(3915)$ (assuming it to be a spin-2 state), and 18 eV for $\chi_{c2}(2P)$. We also report upper limits on the ratios of branching fractions $\mathcal{B}(\eta_c(2S) \to \eta_c\pi^+\pi^-)/\mathcal{B}(\eta_c(2S) \to K^0_S K^+\pi^-) < 10.0$ and $\mathcal{B}(\chi_{c2}(1P) \to \eta_c\pi^+\pi^-)/\mathcal{B}(\chi_{c2}(1P) \to K^0_S K^+\pi^-) < 32.9$ at the 90% confidence level.

PACS numbers: 13.25.Gv, 14.40.Pq

Two-photon fusion events provide a useful production mode to study charmonium states with quantum numbers $J^{PC} = 0^{\pm+}, 2^{\pm+}, 4^{\pm+}, ..., 3^{++}, 5^{++}, ...$ [1, 2]. Dipion transitions among these states have been searched for only in the case of $\eta_c(2S) \to \eta_c\pi^+\pi^-$ [4], in contrast to the narrower vector states, where dipion transitions have been studied extensively. In particular, the transition amplitude for $\eta_c(2S) \to \eta_c\pi^+\pi^-$ [3] is expected [5] to have the same approximately linear dependence on the invariant-mass-squared of the dipion system as the $\psi(2S) \to J/\psi\pi^+\pi^-$ decay [6]. Phase-space integration of the squared amplitude, evaluated for the peak masses M_{η_c} and $M_{\eta_c(2S)}$ [1] of the η_c and $\eta_c(2S)$, respectively, yields $\Gamma(\eta_c(2S) \to \eta_c\pi^+\pi^-)/\Gamma(\psi(2S) \to J/\psi\pi^+\pi^-) \approx 2.9$. This leads to the branching fraction prediction $\mathcal{B}(\eta_c(2S) \to \eta_c\pi^+\pi^-) = (2.2^{+1.6}_{-0.6})\%$, where the uncertainty is due to the uncertainty on the width of the $\eta_c(2S)$ [1]. This decay may be further suppressed due to the contribution of the chromo-magnetic interaction to the decay amplitude [7].

In recent years, experiments have reported evidence for charmonium-like states, such as the $X(3872)$ [8] and $Y(4260)$ [9], which do not fit well into the conventional $c\bar{c}$ picture. This has prompted much theoretical activity and proposals for new models [10]. Several studies of these states have been performed with the $J/\psi\pi^+\pi^-$ final state [11], but no search using the $\eta_c\pi^+\pi^-$ final state has been conducted. Such a search may shed light on the quantum numbers or the internal dynamics of these states. In particular, it has been suggested [12] that if the $X(3872)$ is the 1^1D_2 state η_{c2}, then the branching fraction $\mathcal{B}(X(3872) \to \eta_c\pi^+\pi^-)$ could be significantly larger

*Now at the University of Tabuk, Tabuk 71491, Saudi Arabia
†Also with Università di Perugia, Dipartimento di Fisica, Perugia, Italy
‡Now at the University of Huddersfield, Huddersfield HD1 3DH, UK
§Now at University of South Alabama, Mobile, Alabama 36688, USA
¶Also with Università di Sassari, Sassari, Italy
**Deceased

than $\mathcal{B}(X(3872) \to J/\psi\pi^+\pi^-)$. The quantum numbers $J^{PC} = 2^{-+}$ of the η_{c2} are consistent with the results of an angular analysis of $X(3872) \to J/\psi\pi^+\pi^-$ [13] and would allow production of $X(3872)$ in two-photon fusion.

We present herein a study of the process $\gamma\gamma \to X \to \eta_c\pi^+\pi^-$, where X is one of the resonances $\chi_{c2}(1P)$, $\eta_c(2S)$, $X(3872)$, $X(3915)$, or $\chi_{c2}(2P)$, and the η_c is reconstructed in the final state $K^0_S K^+\pi^-$ [14].

The data sample was collected with the *BABAR* detector at the PEP-II asymmetric-energy e^+e^- collider located at the SLAC National Accelerator Laboratory. It consists of 429.1 ± 1.9 fb^{-1} collected at the energy of the $\Upsilon(4S)$ resonance, constituting the entire *BABAR* $\Upsilon(4S)$ dataset, and 44.8 ± 0.2 fb^{-1} collected about 40 MeV below the $\Upsilon(4S)$ resonance. The *BABAR* detector is described in detail in Ref. [16].

Samples of Monte Carlo (MC) simulated events are analyzed with the same reconstruction and analysis procedures as the data sample, following a `GEANT4`-based [17] detector simulation [16]. Simulated background samples include $e^+e^- \to q\bar{q}$ continuum events ($q = u, d, s, c$) generated with JETSET [18], $\Upsilon(4S) \to B\bar{B}$ decays generated with EvtGen [19] and JETSET, and $e^+e^- \to \tau^+\tau^-$ events generated with KK [20]. In order to study initial-state-radiation (ISR) background and the invariant-mass resolution, a sample of $e^+e^- \to \gamma\psi(2S)$ events with $\psi(2S) \to J/\psi\pi^+\pi^-$ and $J/\psi \to K^0_S K^+\pi^-$ is generated with EvtGen. The GAMGAM [21] generator is used to generate signal event samples for each of the X states studied, with the decay $X \to \eta_c\pi^+\pi^-$ simulated with an amplitude that is uniform throughout the decay phase space, independent of the final-state kinematic variables. The decay $\eta_c \to K^0_S K^+\pi^-$ is generated with a uniform amplitude or with equal and incoherent $K^*_0(1430)^- K^+$ and $\bar{K}^*_0(1430)^0 K^0$ contributions. The GAMGAM generator is also used to generate $\gamma\gamma \to \eta_c \to K^0_S K^+\pi^-$ events.

The analysis is performed with two data samples. The sample used to search for the process $\gamma\gamma \to X \to \eta_c\pi^+\pi^-$ is referred to as the "main sample". Properties of the η_c and its decay into $K^0_S K^+\pi^-$ are studied with a separate "control sample" of $\gamma\gamma \to \eta_c \to K^0_S K^+\pi^-$ events. For the main (control) sample, we select events that contain six (four) charged-particle tracks.

For both samples, charged kaon candidates are identified using likelihood values calculated from measurements of specific energy loss and information from a detector of internally reflected Cherenkov radiation. All other tracks are assumed to be pions. A K^0_S candidate is reconstructed by fitting a $\pi^+\pi^-$ pair to a common vertex, with invariant mass in the range $0.491 < m(\pi^+\pi^-) < 0.503$ GeV/c^2. A kinematic fit is performed, constraining $m(\pi^+\pi^-)$ to the nominal K^0_S mass [22]. An $\eta_c \to K^0_S K^+\pi^-$ decay candidate is reconstructed by combining a K^0_S candidate with a K^+ and a π^- and requiring the resulting invariant mass to lie in the range $2.77 < m(K^0_S K^+\pi^-) < 3.22$ GeV/c^2. In the main sample, the decay $X \to \eta_c\pi^+\pi^-$ is reconstructed by combining an η_c candidate with the remaining two tracks in the event. A kinematic fit is applied, requiring the X-candidate decay vertex to be consistent with the e^+e^- interaction region. The angle $\alpha_{K^0_S}$ between the K^0_S momentum vector and the line connecting the η_c and the K^0_S decay vertices is required to satisfy $\cos\alpha_{K^0_S} > 0.99$.

In the control sample, we require the polar angle (the angle with respect to the beam axis) θ_{η_c} of the η_c candidate to satisfy $|\cos\theta_{\eta_c}| > 0.99$ and the transverse momentum of the η_c candidate to satisfy $p^T_{\eta_c} < 0.5$ GeV/c, both in the center-of-mass (CM) frame of the e^+e^- system. The extra energy in the event, defined as the total energy in calorimeter clusters not associated with the identified tracks, is required to satisfy $E_{\rm ex} < 0.5$ GeV in the CM frame. The $m(K^0_S K^+\pi^-)$ distribution of the selected control-sample events, shown in Fig. 1(a), exhibits clear η_c and J/ψ peaks, with the J/ψ produced in ISR events. In the main sample, continuum background is strongly suppressed with the requirements $|\cos\theta_X| > 0.85$, $p^T_X < 1.5$ GeV/c, and $E_{\rm ex} < 0.8$ GeV, where $\cos\theta_X$ and p^T_X are the polar angle and transverse momentum of the X candidate. In addition, the total visible energy in the event, obtained from all charged tracks and calorimeter clusters, is required to satisfy $E_{vis} < 10$ GeV in the laboratory frame.

In the main sample, we suppress QED background by requiring $R2 < 0.7$, where $R2$ is the ratio of the second and zeroth Fox-Wolfram moments [23]. We suppress background due to ISR events with a requirement on the missing mass squared $m^2_{\rm miss} \equiv (p_{e^+e^-} - p_X)^2 > 10$ GeV$^2/c^4$, where $p_{e^+e^-}$ (p_X) is the total 4-momentum of the beam particles (X candidate).

Additional background suppression in the main sample is obtained by using the Dalitz plot for the η_c candidates. The Dalitz plot is shown in Fig. 1(b) for control-sample events in the η_c peak region $2.94 < m(K^0_S K^+\pi^-) < 3.02$ GeV/c^2, and in Figs. 1(c) and 1(d) for main-sample events in the lower and upper $m(K^0_S K^+\pi^-)$ sidebands $2.8 < m(K^0_S K^+\pi^-) < 2.9$ GeV/c^2 and $3.05 < m(K^0_S K^+\pi^-) < 3.2$ GeV/c^2, respectively. These distributions indicate that true $\eta_c \to K^0_S K^+\pi^-$ decays often proceed via intermediate $K^*_0(1430)$ states, while background events contain $K^*(892)$ decays and random combinations. Taking advantage of this difference to suppress non-η_c background in the main sample, we require $|m^2(K^0_S\pi^-) - M^2_{K^*_0(1430)^-}| < 0.5$ GeV$^2/c^4$ or $|m^2(K^+\pi^-) - M^2_{K^*_0(1430)^0}| < 0.5$ GeV$^2/c^4$, and exclude events that satisfy $|m^2(K^0_S\pi^-) - M^2_{K^*(892)^-}| < 0.35$ GeV$^2/c^4$ or $|m^2(K^+\pi^-) - M^2_{K^*(892)^0}| < 0.2$ GeV$^2/c^4$, where M_R is the peak mass of resonance R [22]. The Dalitz-plot region selected by these criteria is enclosed within the solid lines in Figs. 1(b), 1(c) and 1(d). The criteria are the result of maximizing $\varepsilon^{DP}_{\eta_c}/\sqrt{\varepsilon^{DP}_{SB}}$, where $\varepsilon^{DP}_{\eta_c} = (63.5 \pm 3.2)\%$ is the efficiency of the Dalitz-plot requirements for η_c decays, determined by fitting the $m(K^0_S K^+\pi^-)$ distribution of the control-sample, and

$\varepsilon_{SB}^{DP} = (30.74 \pm 0.21)\%$ is the corresponding efficiency for main-sample events in the $m(K_S^0 K^+ \pi^-)$ sidebands. The $\bar{D}^0 \to K^+\pi^-$ band, evident in Fig. 1(c), becomes insignificant following a neural-network requirement, described below. Therefore, no explicit effort is made to remove this source of background.

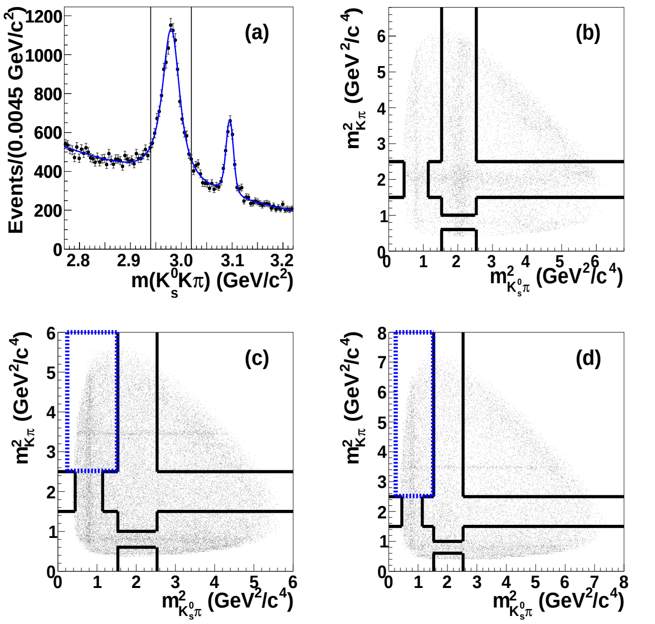

FIG. 1: (a) The $m(K_S^0 K^+ \pi^-)$ distribution for the control sample. The vertical lines indicate the η_c peak mass region. Also shown are the $K_S^0 K^+ \pi^-$ Dalitz-plots for (b) control-sample events in the η_c peak mass region and for main-sample events in the (c) lower and (d) upper η_c mass sidebands. Solid black lines indicate the regions defined by the Dalitz-plot selection criteria. The dotted blue box in the upper left corner of (c) and (d) indicates the Dalitz-plot-sideband background region used for the neural-network training.

Further background suppression is achieved by combining six variables into a neural-network discriminator. Two of the variables are $E_{\rm ex}$ and p_X^T. Each of the remaining four variables is a discrete output value of a kaon- or pion-identification algorithm applied to one of the charged-particle tracks that is not a daughter of the K_S^0 candidate. The distributions of the neural-network input variables are shown in Figs. 2(a–d). The neural network is trained with signal MC and main-sample background events in the Dalitz-plot sideband region $m^2(K^+\pi^-) > 2.5$ GeV$^2/c^4$, $m^2(K_S^0\pi^-) < 1.5$ GeV$^2/c^4$, indicated by the dashed boxes in Figs. 1(c) and 1(d). This region is chosen since it contains only $(3.40 \pm 0.66)\%$ of η_c decays in the control sample. We find only insignificant differences in the neural network signal-to-background separation when using different signal samples or the mirror Dalitz-plot region $m^2(K^+\pi^-) < 1.5$ GeV$^2/c^4$, $m^2(K_S^0\pi^-) > 2.5$ GeV$^2/c^4$ for the background. The distributions of the output variable $V_{\rm NN}$ are shown in Fig. 2(e) for signal and background events. We find the optimal selection on this variable to be $V_{\rm NN} > 0.84$. The signal efficiency of this selection is 72% for the $\eta_c(2S)$, and varies by up to 4%, depending on the X mass. The background efficiency is $(10.4 \pm 0.2)\%$ for the neural-network training region and $(7.4 \pm 0.2)\%$ for the mirror region.

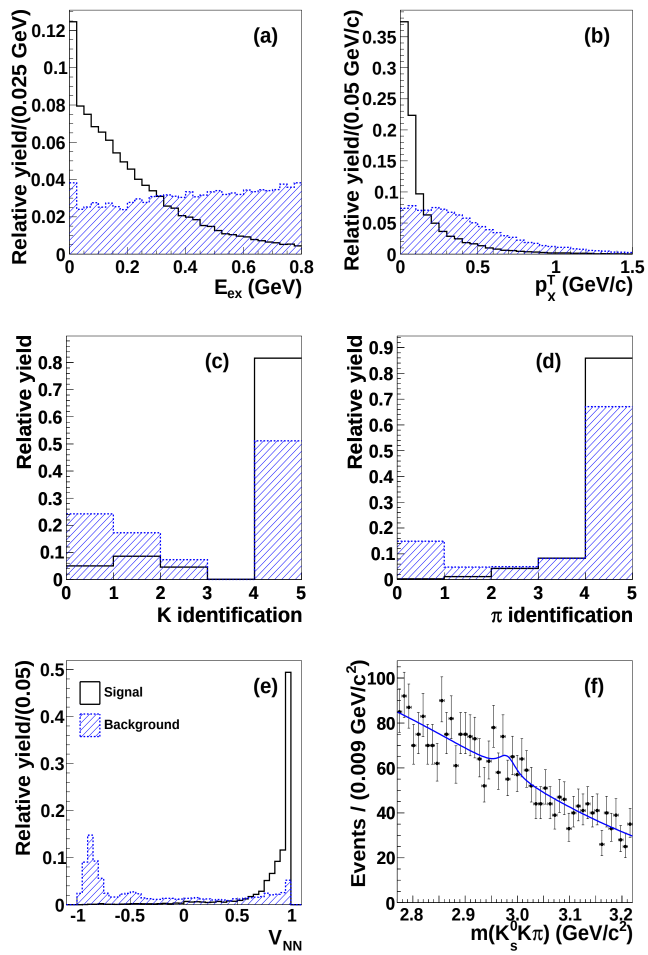

FIG. 2: Signal (unhatched) and background (hatched) distributions of the neural-network input variables (a) $E_{\rm ex}$, (b) p_X^T, and the (c) kaon and (d) pion identification variables. (e) The distributions of the neural-network output variable $V_{\rm NN}$. (f) The $m(K_S^0 K^+ \pi^-)$ distribution of the data with the step-1 fit function overlaid.

We find 2863 main-sample events that satisfy all the selection criteria, with only about 700 events expected from non-$\gamma\gamma$ background MC. We conclude that the majority of the background is due to $\gamma\gamma$ events, for which we have no generic generator. More than one X candidate is reconstructed in 3.8% of the events. In these cases, we select the candidate for which $m^2(K_S^0\pi^-)$ or $m^2(K^+\pi^-)$ is closest to the $K_0^*(1430)$ peak.

In addition to these samples, an ISR-produced sample of $\psi(2S) \to J/\psi \pi^+\pi^-$ events is used to evaluate a systematic uncertainty associated with the detector resolution. This sample is selected in the same way as the main sample, except that the neural-network and Dalitz-plot selections are not applied, the $K_S^0 K^+\pi^-$ invariant mass is required to be between 3.0 and 3.2 GeV/c^2, and $m^2_{\rm miss}$ must be less than 1 GeV$^2/c^4$.

We define four categories of events in the main sample: signal corresponds to $\gamma\gamma \to X \to \eta_c\pi^+\pi^-$ events; combinatorial background (CB), which is by far the most copious background, arises from random combinations of final-state particles; events with a true $\eta_c \to K_S^0 K^+\pi^-$ decay and two pions not originating from an X resonance decay are categorized as η_c-peaking background (η_cB); X-peaking background (XB) corresponds to decays $X \to K_S^0 K^+\pi^-\pi^+\pi^-$ that do not proceed through an intermediate η_c.

The extraction of the signal yield proceeds in two steps. In step 1, we determine the values of the $m(K_S^0 K^+\pi^-)$-distribution parameters of the combinatorial background from a one-dimensional fit to $m(K_S^0 K^+\pi^-)$, without any restrictions on $m(K_S^0 K^+\pi^-\pi^+\pi^-)$.

In step 2, we extract the signal yield for each X resonance hypothesis from a two-dimensional fit to the $m(K_S^0 K^+\pi^-)$ versus $m(K_S^0 K^+\pi^-\pi^+\pi^-)$ distribution for events in an $m(K_S^0 K^+\pi^-\pi^+\pi^-)$ window around the resonance peak. The fits use the unbinned, extended-maximum-likelihood method and are performed with the RooFit package [24].

From events in the $m(K_S^0 K^+\pi^-)$ sidebands, we observe that all correlation between the $m(K_S^0 K^+\pi^-\pi^+\pi^-)$ and $m(K_S^0 K^+\pi^-)$ distributions for the combinatorial background is accounted for by the phase space $\Phi(m(K_S^0 K^+\pi^-), m(K_S^0 K^+\pi^-\pi^+\pi^-))$ of the three-body final state consisting of the π^+, π^-, and the $(K_S^0 K^+\pi^-)$ system. This is used to construct the probability-density function (PDF) [26] of the step-1 fit. This PDF is a function of $m(K_S^0 K^+\pi^-)$ with $m(K_S^0 K^+\pi^-\pi^+\pi^-)$ as a conditional variable, and is given by:

$$\mathcal{H}(m_3|m_5) = N_{\eta_c}\mathcal{H}_{\eta_c}(m_3) + N_{\not\eta_c}\mathcal{H}_{\not\eta_c}(m_3|m_5), \quad (1)$$

where N_{η_c} ($N_{\not\eta_c}$) is the number of events with (without) a true $\eta_c \to K_S^0 K^+\pi^-$ decay. We have used the notation $m_3 \equiv m(K_S^0 K^+\pi^-)$ and $m_5 \equiv m(K_S^0 K^+\pi^-\pi^+\pi^-)$ for brevity.

The PDF for non-η_c events in Eq. (1) is

$$\mathcal{H}_{\not\eta_c}(m_3|m_5) = \mathcal{P}_2(m_3; a_1, a_2, m_3^0)\Phi(m_3, m_5), \quad (2)$$

where $\mathcal{P}_2(m_3; a_1, a_2, m_3^0) = 1 + a_1(m_3 - m_3^0) + a_2(m_3 - m_3^0)^2$ is a second-order polynomial and m_3^0 is a constant offset set to 3.0 GeV/c^2 in order to reduce correlations between a_1 and a_2. Determination of the coefficients a_1, a_2 is the main purpose of the step-1 fit. The PDF for η_c events in Eq. (1) is

$$\mathcal{H}_{\eta_c}(m_3) = \mathcal{W}(m_3; M_{\eta_c}, \Gamma_{\eta_c}, \vec{r}_{m_3}), \quad (3)$$

where $\mathcal{W}$ is a relativistic Breit-Wigner function $\left[(\tilde{m}_3^2 - M_{\eta_c}^2)^2 + M_{\eta_c}^2\Gamma_{\eta_c}^2\right]^{-1}$ convolved with a detector-resolution function $\mathcal{R}(m_3 - \tilde{m}_3; \vec{r}_{m_3})$ that depends on a set of parameters $\vec{r}_{m_3}$ and the difference between the measured m_3 and the true invariant mass $\tilde{m}_3$ of the $K_S^0 K^+\pi^-$ system. The resolution function is the sum of two Crystal Ball functions [25] with oppositely-directed tails and common Gaussian-parameter values,

$$\begin{aligned}\mathcal{R}(x; \vec{r}_x) &= (a_l + a_r)\exp\left[-(x-\bar{x})^2/(2\sigma^2)\right] \\ &+ a_r \times T_r(x) + a_l \times T_l(x),\end{aligned} \quad (4)$$

where

$$T_i(x) = \begin{cases} A_i\left[\sigma/(x_i' - \bar{x})\right]^{n_i} & ; \quad x > \bar{x} + \alpha_i\sigma \\ 0 & ; \quad x \le \bar{x} + \alpha_i\sigma \end{cases} \quad (5)$$

and we have defined $x_i' = x + \sigma(n_i/\alpha_i - \alpha_i)$, and $A_i = (n_i/\alpha_i)^{n_i} \times \exp(-\alpha_i^2/2)$. In Eq. (4), the subscripts r and l label the parameters of the right and left tails, respectively. The values of the resolution-function parameters $\vec{r}_{m_3} = (\bar{x}, \sigma, n_i, \alpha_i, a_i)$ are determined from fits to the signal MC samples.

In addition to a_1 and a_2, the parameter determined in the step-1 fit are the yields N_{η_c} and $N_{\not\eta_c}$, and the mass M_{η_c} and width Γ_{η_c} of the η_c peak. In order to obtain M_{η_c} and Γ_{η_c} from the data, the step-1 fit is performed simultaneously on the main sample and the control sample. The PDF for the control sample is

$$\begin{aligned}\mathcal{H}'(m_3) &= N'_{J/\psi}\mathcal{W}(m_3; M_{J/\psi}, \Gamma_{J\psi}, \vec{r}_{m_3}) \\ &+ N'_{\eta_c}\mathcal{H}_{\eta_c}(m_3) + N'_{\rm bgd}\mathcal{P}_2(m_3; a_1', a_2', m_3^0).\end{aligned} \quad (6)$$

Additional control-sample parameter values determined in the fit are the peak J/ψ mass $M_{J/\psi}$, the background parameters a_1', a_2', and the η_c, J/ψ, and background event yields N'_{η_c}, $N'_{J\psi}$, and $N'_{\rm bgd}$.

The $m(K_S^0 K^+\pi^-)$ distribution of the data and the step-1 PDF are shown in Fig. 2(f). The fitted parameter values are $a_1 = 1.24 \pm 0.19$ (GeV/$c^2)^{-1}$, $a_2 = 0.2 \pm 1.4$ (GeV/$c^2)^{-2}$, $N_{\eta_c} = 50 \pm 37$, $N'_{\eta_c} = 10350 \pm 300$, and $N'_{J/\psi} = 1877 \pm 90$. The large relative uncertainties for a_1 and a_2 are the result of the near linearity of the $m(K_S^0 K^+\pi^-)$ distribution and the correlation between the two parameters, which is taken into account in the evaluation of systematic uncertainties. The η_c parameter values determined in the step-1 fit are $\Gamma_{\eta_c} = 31.7 \pm 1.5$ MeV/c^2 and $M_{\eta_c} = 2.98285 \pm 0.00038$ GeV/c^2, where the uncertainties are statistical only. These results are consistent with previous measurements [22].

The PDF for the step-2 fit is a linear combination of the PDFs of the four event types,

$$\mathcal{P} = N_{\rm sig}\mathcal{P}_{\rm sig} + N_{\rm CB}\mathcal{P}_{\rm CB} + N_{\eta_c{\rm B}}\mathcal{P}_{\eta_c{\rm B}} + N_{X{\rm B}}\mathcal{P}_{X{\rm B}}. \quad (7)$$

The signal PDF is a relativistic Breit-Wigner function convolved with the resolution function, for both m_3 and m_5:

$$\mathcal{P}_{\rm sig}(m_3, m_5) = \mathcal{H}_{\eta_c}(m_3)\,\mathcal{W}(m_5; M_X, \Gamma_X, \vec{r}_{m_5}), \quad (8)$$

where M_X and Γ_X are the known mass and width of the resonance of interest [1, 15, 22], and $\vec{r}_{m_5}$ are the parameters of the $m(K_S^0 K^+\pi^-\pi^+\pi^-)$ resolution function

$\mathcal{R}(m_5 - \tilde{m}_5; \vec{r}_{m_5})$, obtained from a fit to signal MC. The combinatorial-background PDF is

$$\mathcal{P}_{\rm CB}(m_3, m_5) = \mathcal{H}_{\not\eta_c}(m_3|m_5)\, \mathcal{C}_2(m_5; b_1^{\rm CB}, b_2^{\rm CB}), \qquad (9)$$

where $\mathcal{C}_2(m_5; b_1^{\rm CB}, b_2^{\rm CB})$ is a second-order Chebychev polynomial with first- (second-) order coefficients $b_1^{\rm CB}$ ($b_2^{\rm CB}$). The η_c-peaking background PDF is

$$\mathcal{P}_{\eta_c{\rm B}}(m_3, m_5) = \mathcal{H}_{\eta_c}(m_3)\, \mathcal{C}_1(m_5; b_1^{\eta_c{\rm B}}), \qquad (10)$$

where $\mathcal{C}_1(m_5; b_1^{\eta_c{\rm B}})$ is a first-order Chebychev polynomial. The X-peaking background PDF is

$$\begin{aligned} \mathcal{P}_{\rm XB}(m_3, m_5) \;&=\; \mathcal{P}_1(m_3; c_1^{\rm XB}, m_3^0) \\ &\quad\; \mathcal{W}(m_5; M_X, \Gamma_X, \vec{r}_{m_5}), \end{aligned} \qquad (11)$$

where $\mathcal{P}_1(m_3; c_1^{\rm XB}, m_3^0)$ is a first-order polynomial. The parameter values determined with the step-2 fit are the four yields of Eq. (7) and the background shape parameters $b_1^{\rm CB}$, $b_2^{\rm CB}$, $b_1^{\eta_c{\rm B}}$, and $c_1^{\rm XB}$.

The step-2 fit is performed four times in different $m(K^0_S K^+\pi^-\pi^+\pi^-)$ windows, fitting for the (1) $\chi_{c2}(1P)$, (2) $\eta_c(2S)$, (3) $X(3872)$ and $X(3915)$, or (4) $X(3872)$ and $\chi_{c2}(2P)$ resonances. A simultaneous fit to the three resonances $X(3872)$, $X(3915)$, and $\chi_{c2}(2P)$ is observed to be unstable when tested with parametrized MC experiments, due to the large number of fit parameters, small signal, and large overlap of the $X(3915)$ and $\chi_{c2}(2P)$ lineshapes. Therefore, we conduct fits (3) and (4) separately to test for the existence of a signal for either set of lineshape parameters. The $m(K^0_S K^+\pi^-\pi^+\pi^-)$ and $m(K^0_S K^+\pi^-)$ distributions and fit functions are shown in Fig. 3. The difference between the fit function of fit (3) and that of fit (4) is almost indistinguishable within the thickness of the curve in Fig. 3(f). The fitted signal yields are summarized in Table I.

No significant signal or peaking background is observed in any of the fits. However, a hint of X-peaking background is visible in the $\chi_{c2}(1P)$ and $\eta_c(2S)$ fits of Figs. 3(b) and (d), with event yields of 33±14 and 47±24, respectively, where the uncertainties are statistical only. This may be due to decays of $\chi_{c2}(1P)$ and $\eta_c(2S)$ into $K^0_S K^+\pi^-\pi^+\pi^-$ [27], which are suppressed in this analysis by the $2.77 < m(K^0_S K^+\pi^-) < 3.22$ GeV/c^2 requirement. Fits (3) and (4) yield insignificant X-peaking background, roughly canceling the negative signal yields. The results shown in Table I for the $X(3872)$ are obtained from fit (4). The $X(3872)$ yield from fit (3) is 1.6 events lower than in fit (4). Since no signal is observed for the $X(3915)$ or the $\chi_{c2}(2P)$, we obtain a conservative upper limit on the yield of the $X(3915)$ ($\chi_{c2}(2P)$) by fixing the $\chi_{c2}(2P)$ ($X(3915)$) yield to zero.

We estimate systematic uncertainties on the signal yields associated with the fit procedure by repeating the fits with the variations described below and adding the different uncertainties in quadrature. We account for uncertainties in the X mass and width values by varying them within their uncertainties [22]. This is the

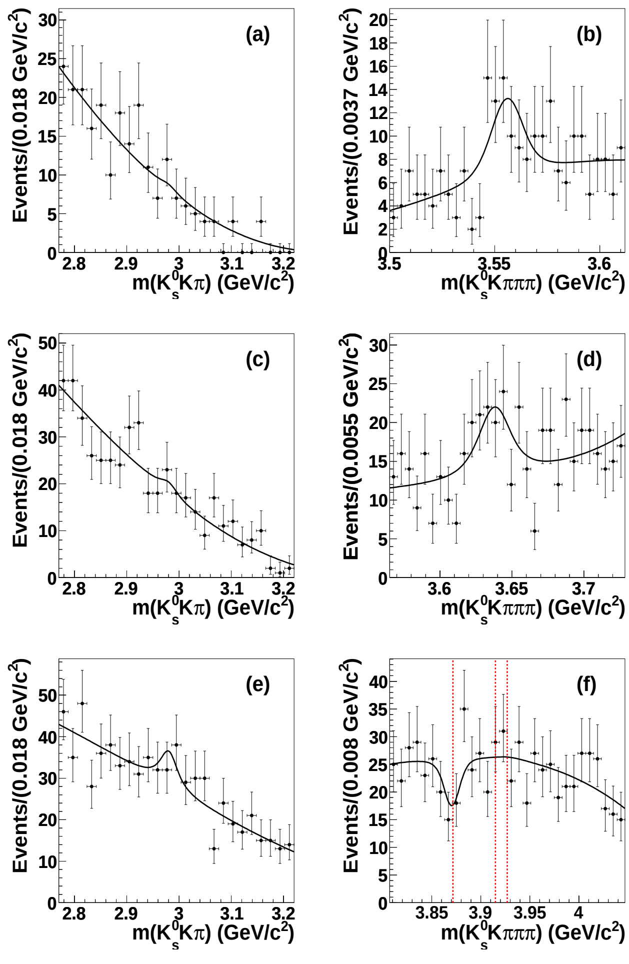

FIG. 3: Distributions of (a,c,e) $m(K^0_S K^+\pi^-)$ and (b,d,f) $m(K^0_S K^+\pi^-\pi^+\pi^-)$ with the step-2 fit PDF overlaid for the fit regions of the (a,b) $\chi_{c2}(1P)$, (c,d) $\eta_c(2S)$, and (e,f) $X(3872)$, $X(3915)$ and $\chi_{c2}(2P)$. The vertical dashed lines in (f) indicate the peak mass positions of the $X(3872)$, $X(3915)$, and $\chi_{c2}(2P)$ [22].

source of the largest signal-yield systematic uncertainty, except for the $\chi_{c2}(1P)$. The order of the polynomial in each PDF is varied to account for uncertainties due to background modeling. We vary the resolution-function Gaussian width (σ in Eq. (4)) by 2 MeV/c^2 for the $m(K^0_S K^+\pi^-)$ PDF to account for a difference between the J/ψ mass resolution in MC and in the control sample, and by 0.9 MeV/c^2 for the $m(K^0_S K^+\pi^-\pi^+\pi^-)$ PDF due to a difference in the $\psi(2S)$ mass resolution between MC and data. An additional uncertainty is evaluated by using the sum of three Gaussians to define the resolution function. To address the possibility that correlations between the m_5 and m_3 distributions are not taken fully into account by the phase-space factor $\Phi(m_3, m_5)$ in Eq. (2), we replace the parameters a_i of Eq. (2) by $a_i(1 + a_i'' m_5)$. The values of the parameters a_i'' are found to be consistent with zero, and we conservatively use their uncertainties to evaluate the systematic uncertainty on the signal yield. The effect of not accounting for phase-space correlations between m_3 and m_5 in the signal and η_c-peaking background PDFs is determined to be small compared to other systematic uncertainties, except for the $\chi_{c2}(1P)$, for which this uncertainty is dominant and equals 2.4 events. Statistical uncertainties from the step-1 fit are propagated to the step-2 fit, accounting for correlations among the parameters.

We test the entire fit procedure using parameterized MC experiments generated with the PDFs of Eqs. (1) and (7). A bias of up to two events on the signal yield is found and used as a correction that is accounted for in the values shown in Table I. A systematic uncertainty on this correction is evaluated by repeating this study after varying the generated signal yield by its statistical uncertainty in the data fit.

Since the dominant combinatorial background is distributed in phase space differently from signal and often contains additional final-state particles, interference between signal and background is expected to be relatively small. In addition, the small signal yields make the evaluation of such interference effects unreliable. Therefore, we do not attempt to account for possible interference.

We evaluate systematic uncertainties on track and K^0_S reconstruction efficiencies, accounting for the momentum and angular distribution of signal tracks, as well as on the uncertainty of the Dalitz-plot requirement efficiency. A 2% systematic uncertainty is assigned due to differences between the distributions of the selection variables in the control sample and in $\gamma\gamma \to \eta_c \to K^0_S K^+\pi^-$ MC. Differences between the data and MC distributions of the particle-identification variables are studied using a high-purity sample of $D^{*+} \to \pi^+ D^0$, $D^0 \to K^-\pi^+$ events, and found to have negligible impact on the efficiency.

The expected Dalitz-plot dependence of the $X \to \eta_c\pi^+\pi^-$ decay is unknown. However, we account for uncertainties in this amplitude, which is uniform in our simulated signal samples, by weighting events according to $\left(m^2(\pi\pi) - 4M_\pi^2\right)^2$ [5], where $m^2(\pi\pi)$ is the squared dipion mass and M_π is the π^- mass. From the weighted sample, we extract an efficiency correction of up to 4.6% (incorporated into the values in Table I) and a systematic uncertainty of the same magnitude.

Finally, we account for a 0.45% uncertainty on the integrated luminosity, for the uncertainties on the K^0_S, η_c, and $\eta_c(2S)$ branching fractions [22], and for MC-statistical uncertainties.

The results are summarized in Table I. From the signal yield $N_{\rm sig}$ of each resonance, the integrated luminosity L, and the signal efficiency ε, we compute the product $\sigma\mathcal{B} = N_{\rm sig}/(L\varepsilon)$ of the $e^+e^- \to Xe^+e^-$ production cross section and the $X \to \eta_c\pi^+\pi^-$ branching fraction. We also evaluate the results in terms of the product $\Gamma_{\gamma\gamma}\mathcal{B}$, where $\Gamma_{\gamma\gamma}$ is the two-photon width of the resonance, by utilizing the GAMGAM generator to determine the cross section as a function of $\Gamma_{\gamma\gamma}$. A 4% uncertainty is assigned to the GAMGAM calculation [2]. Since we find no significant signal for the X resonances, we calculate 90% confidence-level (CL) Bayesian upper limits on these quantities, assuming a Gaussian likelihood incorporating statistical and systematic uncertainties.

Using the efficiency-corrected yields for the χ_{c2} and $\eta_c(2S)$ from [1], we find the relative branching fractions

$$\frac{\mathcal{B}(\eta_c(2S) \to \eta_c\pi^+\pi^-)}{\mathcal{B}(\eta_c(2S) \to K^0_S K^+\pi^-)} = 4.9^{+3.5}_{-3.3} \pm 1.3 \pm 0.8, \quad (12)$$
$$\frac{\mathcal{B}(\chi_{c2}(1P) \to \eta_c\pi^+\pi^-)}{\mathcal{B}(\chi_{c2}(1P) \to K^0_S K^+\pi^-)} = 14.5^{+10.9}_{-8.9} \pm 7.3 \pm 2.5,$$

where the first uncertainty is statistical, the second is systematic, and the third is due to the uncertainty on $\mathcal{B}(\eta_c \to K^0_S K^+\pi^-)$ [22]. The 90% CL upper limits on the two ratios in Eqs. (12) are 10.0 and 32.9, respectively. Using $\mathcal{B}(\eta_c(2S) \to K^0_S K^+\pi^-)$ and $\mathcal{B}(\chi_{c2}(1P) \to K^0_S K^+\pi^-)$ from Ref. [22], we obtain the 90% CL upper limits $\mathcal{B}(\eta_c(2S) \to \eta_c\pi^+\pi^-) < 7.4\%$ and $\mathcal{B}(\chi_{c2}(1P) \to \eta_c\pi^+\pi^-) < 2.2\%$.

In summary, we report a study of the process $\gamma\gamma \to \eta_c\pi^+\pi^-$ and provide, for the first time, upper limits on the branching fractions of $\chi_{c2}(1P)$ and $\eta_c(2S)$ decays to $\eta_c\pi^+\pi^-$ relative to the branching fractions of the decays into $K^0_S K^+\pi^-$. We also report upper limits on the products $\sigma\mathcal{B}$ and $\Gamma_{\gamma\gamma}\mathcal{B}$ for the $\chi_{c2}(1P)$, $\eta_c(2S)$, $X(3872)$, $X(3915)$, and $\chi_{c2}(2P)$ resonances.

TABLE I: Results of the step-2 fits. For each resonance X, we show the peak mass and width used in the PDF (from Refs. [1, 15, 22]); the mass range of the fit; the efficiency; the bias-corrected signal yield with statistical and systematic uncertainties; the product of the $\gamma\gamma \to X$ production cross section and $X \to \eta_c \pi^+ \pi^-$ branching fraction, and the 90% CL upper limit (UL) on this product; the product of the two-photon partial width $\Gamma_{\gamma\gamma}$ and the $X \to \eta_c \pi^+ \pi^-$ branching fraction, and the 90% CL upper limit on this product. For the $X(3872)$ and the $X(3915)$ we assume $J = 2$.

Resonance	M_X (MeV/c^2)	Γ_X (MeV)	m_5 Range (GeV/c^2)	ε (%)	N_{sig}	$\sigma\mathcal{B}$(fb)		$\Gamma_{\gamma\gamma}\mathcal{B}$(eV)	
						Central value	UL	Central value	UL
$\chi_{c2}(1P)$	3556.20 ± 0.09	1.97 ± 0.11	3.500-3.612	3.60 ± 0.39	$10.2^{+7.7}_{-6.3} \pm 3.5$	$37^{+28}_{-23} \pm 15$	80	$7.2^{+5.5}_{-4.4} \pm 2.9$	15.7
$\eta_c(2S)$	3638.5 ± 1.7	13.4 ± 5.6	3.565-3.728	3.53 ± 0.35	$17^{+12}_{-11} \pm 3$	$61^{+44}_{-41} \pm 16$	123	$65^{+47}_{-44} \pm 18$	133
$X(3872)$	3871.57 ± 0.25	3.0 ± 2.1	3.807-4.047	3.92 ± 0.38	$-4.7^{+7.9}_{-6.9} \pm 2.8$	$-16^{+26}_{-23} \pm 10$	38	$-4.5^{+7.7}_{-6.7} \pm 2.9$	11.1
$X(3915)$	3915.0 ± 3.6	17.0 ± 10.4	3.807-4.047	3.79 ± 0.37	$-13^{+11}_{-11} \pm 7$	$-44^{+38}_{-38} \pm 25$	53	$-13^{+12}_{-12} \pm 8$	16
$\chi_{c2}(2P)$	3927.2 ± 2.6	24 ± 6	3.807-4.047	3.75 ± 0.36	$-15^{+14}_{-13} \pm 4$	$-53^{+49}_{-46} \pm 18$	60	$-16^{+15}_{-14} \pm 6$	18

We are grateful for the extraordinary contributions of our PEP-II colleagues in achieving the excellent luminosity and machine conditions that have made this work possible. The success of this project also relies critically on the expertise and dedication of the computing organizations that support *BABAR*. The collaborating institutions wish to thank SLAC for its support and the kind hospitality extended to them. This work is supported by the US Department of Energy and National Science Foundation, the Natural Sciences and Engineering Research Council (Canada), the Commissariat à l'Energie Atomique and Institut National de Physique Nucléaire et de Physique des Particules (France), the Bundesministerium für Bildung und Forschung and Deutsche Forschungsgemeinschaft (Germany), the Istituto Nazionale di Fisica Nucleare (Italy), the Foundation for Fundamental Research on Matter (The Netherlands), the Research Council of Norway, the Ministry of Education and Science of the Russian Federation, Ministerio de Ciencia e Innovación (Spain), and the Science and Technology Facilities Council (United Kingdom). Individuals have received support from the Marie-Curie IEF program (European Union), the A. P. Sloan Foundation (USA), and the Binational Science Foundation (USA-Israel).

[1] P. del Amo Sanchez *et al.* (*BABAR* Collaboration), Phys. Rev. D **84**, 012004 (2011).
[2] B. Aubert *et al.* (*BABAR* Collaboration), Phys. Rev. D **81**, 092003 (2010).
[3] We refer to the $\eta_c(1S)$ as η_c.
[4] D. Cronin-Hennessy *et al.* (CLEO Collaboration), Phys. Rev. D **81**, 052002 (2010).
[5] M. B. Voloshin, Mod. Phys. Lett. A **17**, 1533 (2002).
[6] J.Z. Bai *et al.* (BES Collaboration), Phys. Rev. D **62**, 032002 (2000).
[7] M. B. Voloshin, Phys. Rev. D **74**, 054022 (2006).
[8] S. K. Choi *et al.* (Belle Collaboration), Phys. Rev. Lett. **91**, 262001 (2003).
[9] B. Aubert *et al.* (*BABAR* Collaboration), Phys. Rev. Lett. **95**, 142001 (2005); B. Aubert *et al.* (*BABAR* Collaboration), Phys. Rev. Lett. **98**, 212001 (2007).
[10] E.S. Swanson, Phys. Rept. **429**, 243 (2006); N.A. Tornqvist, Phys. Lett. B **590**, 209 (2004); L. Maiani, V. Riquer, F. Piccinini and A. D. Polosa, Phys. Rev. D **72**, 031502 (2005).
[11] B. Aubert *et al.* (*BABAR* Collaboration), Phys. Rev. Lett. **95**, 142001 (2005); C. Z. Yuan *et al.* (Belle Collaboration), Phys. Rev. Lett. **99**, 182004 (2007); D. Acosta *et al.* (CDF Collaboration), Phys. Rev. Lett. **93**, 072001 (2004); V.M. Abazov *et al.* (DØCollaboration), Phys. Rev. Lett. **93**, 162002 (2004); S. Dobbs *et al.* (CLEO Collaboration), Phys. Rev. Lett. **94**, 032004 (2005).
[12] S. Olsen *et al.* (Belle Collaboration), Int. J. Mod. Phys. A **20**, 240 (2005).
[13] A. Abulencia *et al.* (CDF Collaboration), Phys. Rev. Lett. **98**, 132002 (2007).
[14] The use of charge conjugate reactions is implied throughout this paper.
[15] S. Uehara *et al.* (Belle Collaboration), Phys. Rev. Lett. **104**, 092001 (2010).
[16] B. Aubert *et al.* (*BABAR* Collaboration), Nucl. Instrum. Meth. A **479**, 1 (2002).
[17] S. Agostinelli *et al.* (Geant4 Collaboration), Nucl. Instrum. Methods Phys. Res., Sect. A **506**, 250 (2003).
[18] T. Sjöstrand, Comput. Phys. Commun. **82**, 74 (1994).
[19] D. Lange, Nucl. Instrum. Methods Phys. Res., Sect. A **462**, 152 (2001).
[20] S. Jadach, B. F. L. Ward and Z. Was, Nucl. Phys. Proc. Suppl. **89**, 106 (2000).
[21] V. M. Budnev, I. F. Ginzburg, G. V. Meledin and V. G. Serbo, Phys. Rept. **15** (1975) 181.
[22] K. Nakamura *et al.* (Particle Data Group), J. Phys. G **37**, 075021 (2010), and partial update for the 2012 edition (URL: http://pdg.lbl.gov).
[23] G.C. Fox and S. Wolfram, Nucl. Phys. B **149**, 413 (1979).
[24] All fits are performed with the RooFit package, W. Verkerke and D. P. Kirkby, *Proceedings of the 2003 Conference for Computing in High-Energy and Nuclear Physics (CHEP 03), La Jolla, California, 24-28 Mar 2003, pp MOLT007*.
[25] M. J. Oreglia, Ph.D. thesis, Report No. SLAC-R-236, 1980; J. E. Gaiser, Ph.D. thesis, Report No. SLAC-R-255, 1982; T. Skwarnicki, Ph.D. thesis, Report No. DESY F31-86-02, 1986.
[26] All PDFs include implicit normalization coefficients that are not mentioned.
[27] H. Nakazawa (Belle Collaboration), PoS **ICHEP2010**, 162 (2010).